LETTER

doi:10.1038/nature13158

Maternal retinoids control type 3 innate lymphoid cells and set the offspring immunity

Serge A. van de Pavert[1]†*, Manuela Ferreira[2]*, Rita G. Domingues[2], Hélder Ribeiro[2], Rosalie Molenaar[1], Lara Moreira-Santos[2], Francisca F. Almeida[2], Sales Ibiza[2], Inês Barbosa[2], Gera Goverse[1], Carlos Labão-Almeida[2], Cristina Godinho-Silva[2], Tanja Konijn[1], Dennis Schooneman[1], Tom O'Toole[1], Mark R. Mizee[1], Yasmin Habani[1], Esther Haak[3], Fabio R. Santori[4], Dan R. Littman[4], Stefan Schulte-Merker[5], Elaine Dzierzak[3], J. Pedro Simas[2], Reina E. Mebius[1]* & Henrique Veiga-Fernandes[2]*

The impact of nutritional status during fetal life on the overall health of adults has been recognized[1]; however, dietary effects on the developing immune system are largely unknown. Development of secondary lymphoid organs occurs during embryogenesis and is considered to be developmentally programmed[2,3]. Secondary lymphoid organ formation depends on a subset of type 3 innate lymphoid cells (ILC3) named lymphoid tissue inducer (LTi) cells[2–5]. Here we show that mouse fetal ILC3s are controlled by cell-autonomous retinoic acid (RA) signalling *in utero*, which pre-sets the immune fitness in adulthood. We found that embryonic lymphoid organs contain ILC progenitors that differentiate locally into mature LTi cells. Local LTi cell differentiation was controlled by maternal retinoid intake and fetal RA signalling acting in a haematopoietic cell-autonomous manner. RA controlled LTi cell maturation upstream of the transcription factor RORγt. Accordingly, enforced expression of *Rorgt* restored maturation of LTi cells with impaired RA signalling, whereas RA receptors directly regulated the *Rorgt* locus. Finally, we established that maternal levels of dietary retinoids control the size of secondary lymphoid organs and the efficiency of immune responses in the adult offspring. Our results reveal a molecular link between maternal nutrients and the formation of immune structures required for resistance to infection in the offspring.

Haematopoietic cells that initially colonize secondary lymphoid organ (SLO) sites include $CD3^-$c-$Kit^+$$IL\text{-}7R\alpha^-\alpha4\beta7^+CD11c^+CD4^-$ lymphoid tissue initiator (LTin) cells and the prototypical member of type 3 ILCs, LTi cells[2–7]. Although most LTi cells express CD4, this is a late event in LTi differentiation and not all $ROR\gamma t^+$ LTi cells express this marker[5,6,8,9]. Thus, we proposed that $CD3^-IL\text{-}7R\alpha^+\alpha4\beta7^+ID2^+$c-$Kit^+$$CD11c^-CD4^-$ ILCs (hereafter called ILC_{4neg} cells) receive local cues giving rise to $ID2^+ROR\gamma t^+CD4^+$ LTi cells (LTi_4) within developing SLOs. Notably, enteric ILC_{4neg} cells include mainly $ID2^+ROR\gamma t^+CD4^-$ LTi cells (LTi_0) but also a small fraction of $ID2^+ROR\gamma t^-CD4^-$ precursors with LTi cell potential (hereafter called pre-ILC cells)[9]. In contrast, nearly 100% of lymph node ILC_{4neg} cells are LTi_0 cells (Extended Data Fig. 1a, b). Analysis of embryonic day 12.5 (E12.5) guts revealed that ILC_{4neg} cells are the only appreciable $IL\text{-}7R\alpha^+$ colonizing cells (Fig. 1a, b). Accordingly, non-cycling mature $Sca1^-$ LTi_4 cells increased throughout development, seemingly at the expense of $Sca1^+$ ILC_{4neg} cells (Fig. 1a–c and Extended Data Fig. 1c). Further evidence that ILC_{4neg} cells differentiate locally was provided by organ cultures and transplantation of E12.5 intestines. Despite absence of fetal liver output in these settings, LTi_4 cells increased with time at the expense of local ILC_{4neg} cells (Fig. 1d, e). Furthermore, in E14.5 $Rorgt^{-/-}$ embryos, ILC_{4neg} cells were attracted to the intestine and lymph nodes, supporting initial anlagen colonization by these cells (Extended Data Fig. 1d, e). Notably, RA stimulation of E13.5 lymph node cells showed increased frequency of LTi_4 cells and reduction of ILC_{4neg} cells, indicating that differentiation of LTi_4 cells is regulated by RA (Fig. 1f). To confirm the effect of RA in LTi differentiation *in vivo*, pregnant mice received a RA-enriched diet starting at E10.5. Supplementation of RA increased the proportion of LTi_4 cells in the embryo, to the detriment of ILC_{4neg} cells (Fig. 1f). In agreement with this finding, provision of the RA signalling inhibitor BMS493 to pregnant female mice resulted in a decrease of fetal LTi_4 cells despite normal frequency of fetal liver progenitors and enteric haematopoietic cells (Fig. 1f and Extended Data Fig. 1f). Consequently, despite normal embryo size, BMS493 administration led to a reduction in lymph node dimensions and Peyer's patch developmental failure (Fig. 1g–i and Extended Data Fig. 1g). Collectively, our data indicate that maternal retinoids control LTi cell differentiation within developing SLOs.

RA is a vitamin A metabolite that controls early vertebrate development, some immune processes in adulthood, and has been shown to mediate CXCL13 expression in fetal mesenchymal cells[10–16]. RA binds to heterodimers formed by the RA receptors (RARs) and retinoid X receptors (RXRs), which bind DNA RA response elements (RAREs)[11]. To address putative RA cell-autonomous responses, we assessed RAR and RXR expression in E15.5 ILC_{4neg}, LTi_4 and LTin cells. RARs and RXRs were predominantly expressed by ILC_{4neg} and LTi_4 cells, whereas LTin cells expressed these molecules at lower levels (Fig. 2a). RA stimulation revealed that only ILC_{4neg} and LTi_4 cells respond robustly, as shown by *Rarb* upregulation (Fig. 2b)[16]. Together, these data indicate that impaired SLO development in BMS493-treated mice might be the consequence of RA signal ablation in LTi cells. To test this hypothesis we used a lineage-targeted model to block RA signalling. We used a mouse line in which a truncated form of the RARα gene was knocked into the *ROSA26* locus preceded by a triple polyadenylation signal flanked by two *loxP* sites (*ROSA26*-RARα403). This line was bred to *Vav*-iCre mice that in contrast to other tested Cre lines ensured Cre activity in fetal LTin, ILC_{4neg} and LTi_4 cells (Extended Data Fig. 2a–d)[17,18]. Despite normal frequencies of fetal liver precursors, and SLO LTin, ILC_{4neg} and LTi_0 cells, *Vav*-iCre/*ROSA26*-RARα403 embryos (Rar mice) revealed a dose-dependent reduction of LTi_4 cells (Fig. 2c, d and Extended Data Fig. 3a–f). To assess whether the differentiation potential of ILC_{4neg} cells is controlled by RA thresholds, we cultured purified ILC_{4neg} cells from Rar heterozygous (Rar^{Het}), homozygous (Rar^{Hom}) and wild-type littermate control mice. Whereas wild-type ILC_{4neg} cells upregulated pro-inflammatory cytokines and chemokines and gave rise to LTi_4 cells *in vitro*, these were impaired proportionally to the degree of RA signalling abrogation in ILC_{4neg} cells (Fig. 2e, f and Extended Data Fig. 3g). Finally, despite normal frequency of colonizing ILC_{4neg} cells (Fig. 2d),

[1]Department of Molecular Cell Biology and Immunology, VU University Medical Center, van der Boechorststraat 7, 1081BT Amsterdam, The Netherlands. [2]Instituto de Medicina Molecular, Faculdade de Medicina de Lisboa, Av. Prof. Egas Moniz, Edifício Egas Moniz, 1649-028 Lisboa, Portugal. [3]Erasmus Stem Cell Institute, Department of Cell Biology, Erasmus Medical Center, 3000 CA Rotterdam, The Netherlands. [4]Howard Hughes Medical Institute, Molecular Pathogenesis Program, Skirball Institute of Biomolecular Medicine, New York University School of Medicine, New York, New York 10016, USA. [5]Hubrecht Institute–KNAW (Royal Netherlands Academy of Arts and Sciences) and University Medical Center Utrecht, 3584 CT Utrecht, Netherlands. †Present address: Hubrecht Institute–KNAW (Royal Netherlands Academy of Arts and Sciences) and University Medical Center Utrecht, 3584 CT Utrecht, Netherlands.
*These authors contributed equally to this work.

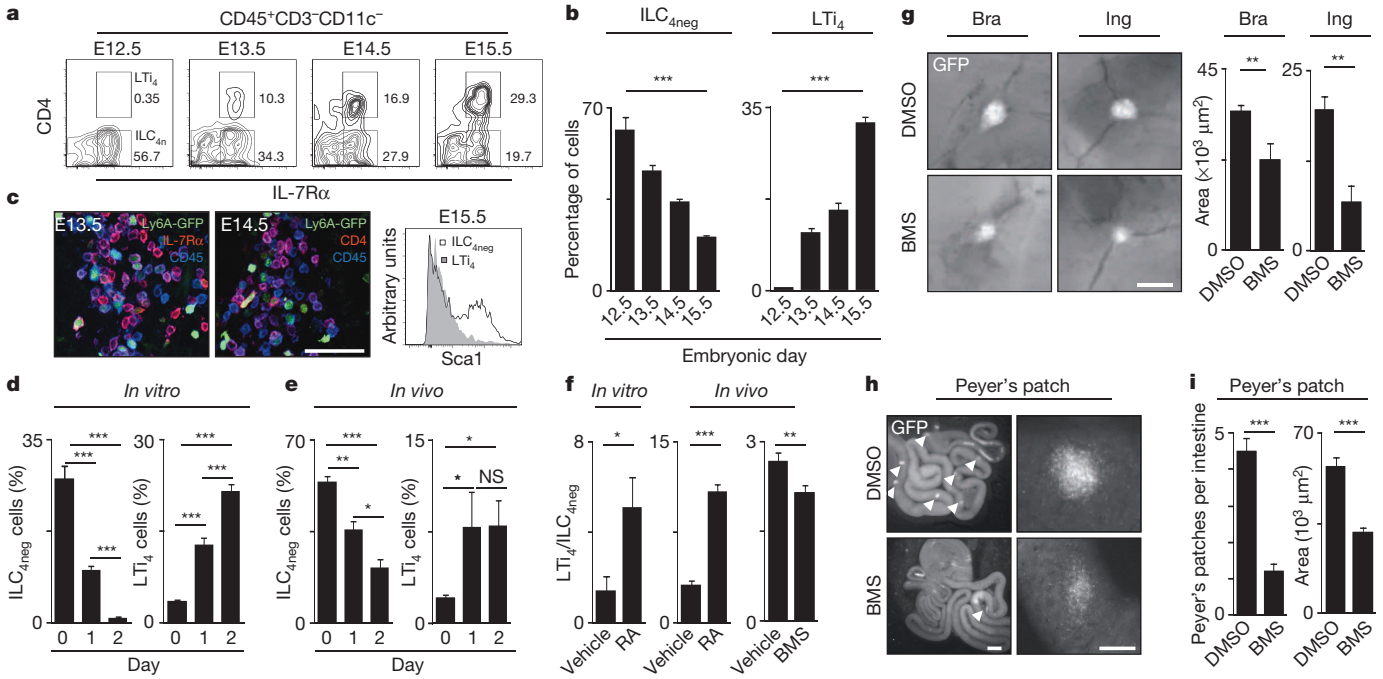

Figure 1 | Maternal RA controls LTi differentiation. **a**, Enteric fetal ILC_{4neg} and LTi_4 cells. **b**, Percentage of enteric fetal ILC_{4neg} and LTi_4 cells. E12.5, $n = 8$; E13.5, $n = 3$; E14.5, $n = 6$; E15.5, $n = 3$. **c**, Left: *Sca1-GFP* lymph nodes. Right: E15.5 gut cells. **d**, **e**, Cultured or transplanted E12.5 guts. **d**, Day 0, $n = 4$; day 1, $n = 6$; day 2, $n = 6$. **e**, Day 0, $n = 7$; day 1, $n = 3$; day 2, $n = 5$. **f**, Left: E13.5 lymph node cells; $n = 7$. Centre: RA was provided to females. E13.5 lymph node cells; $n = 8$. Right: females received BMS493; $n = 8$. LTi_4/ILC_{4neg} cell ratio is shown. **g**–**i**, *hCD2-GFP* females received BMS493. E17.5 SLOs. **g**, Brachial (Bra) and inguinal (Ing) lymph nodes; $n = 6$. **h**, Arrowheads indicate Peyer's patch. **i**, Peyer's patch number per intestine: DMSO, $n = 8$; BMS, $n = 22$. Area: DMSO, $n = 30$; BMS, $n = 25$. Scale bars: 50 μm (**c**), 200 μm (**g**, **h** right), 1 mm (**h**, left). Error bars show s.e. $*P < 0.05$; $**P < 0.01$; $***P < 0.001$. NS, not significant.

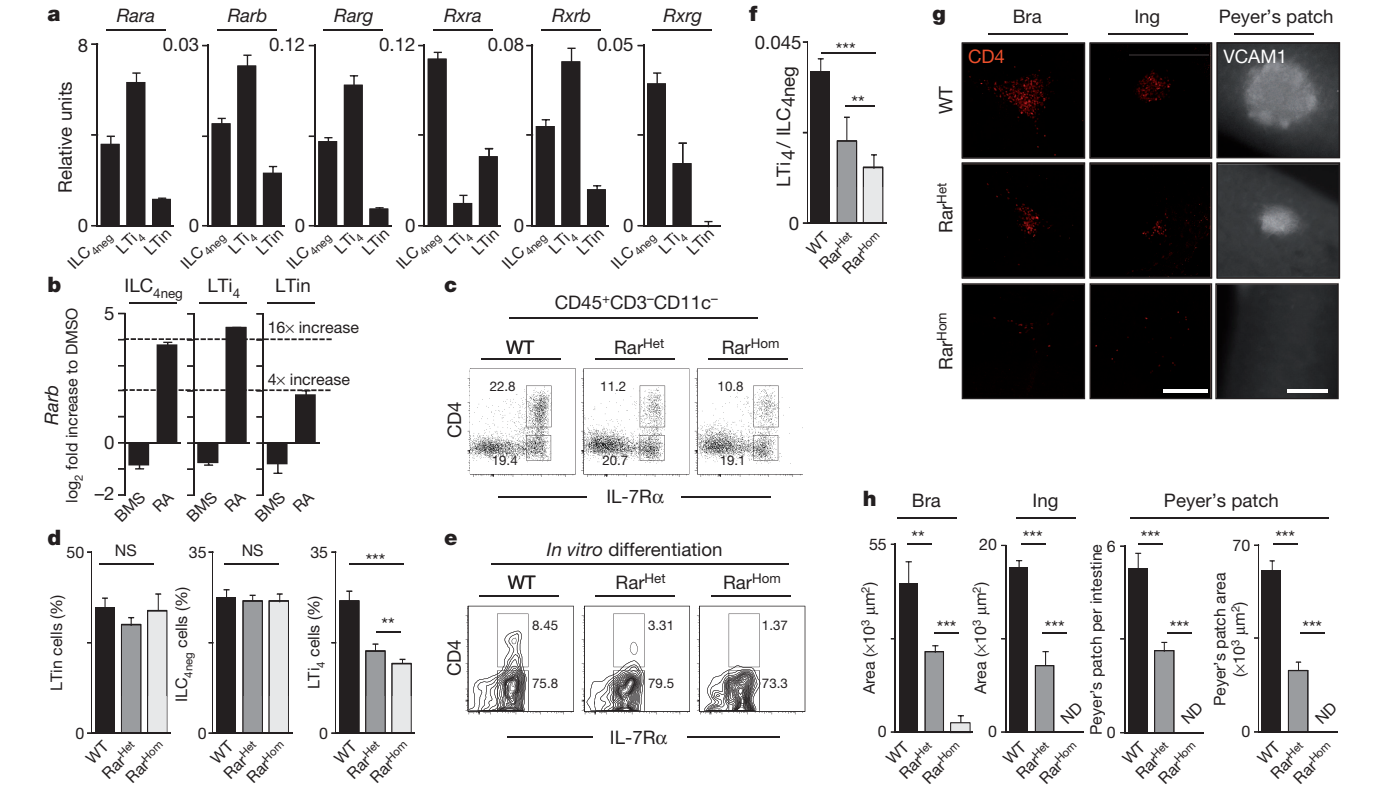

Figure 2 | Cell-autonomous RA controls LTi cells and SLO development. **a**, RT–PCR of enteric cells. Data represent three independent experiments. **b**, DMSO, BMS493 or RA stimulation. Data represent three independent experiments. **c**, E15.5 enteric ILC subsets. **d**, LTin, $n = 4$; ILC_{4neg}, $n = 5$; LTi_4, $n = 5$. **e**, E15.5 ILC_{4neg} cells cultured for 6 days. **f**, ILC_{4neg} cell cultures at day 6; $n = 5$. **g**, Immunostaining of E15.5 embryos and intestines. Developing brachial (Bra) and inguinal (Ing) lymph nodes and Peyer's patch are shown. CD4, red; VCAM1, grey. Scale bars: 200 μm. **h**, SLO size; $n = 6$. Error bars show s.e. $*P < 0.05$; $**P < 0.01$; $***P < 0.001$. NS, not significant. ND, not detected.

haematopoietic cell-autonomous impairment of RA responses resulted in severely diminished fetal lymph node size and reduced number of minute Peyer's patches (Fig. 2g, h and Extended Data Fig. 3h). Our data indicate that LTi cell differentiation is controlled by cell-autonomous RA signalling in developing SLOs.

Previous reports have identified key LTi cell regulators[2]. Mice mutant for the transcription factors ID2 and RORγt lack LTi cells and do not develop SLOs[19,20]. *Runx1*, *Tox* and *Notch1* were also implicated in LTi cell maturation[9,21–23]. We found that whereas most LTi-related genes were normally expressed in Rar^{Hom} and Rar^{Het} ILC_{4neg} and LTi_4 cells, *Runx1* was increased and *Rorgt* was reduced (Fig. 3a and Extended Data Fig. 4a–d). Expression of pro-inflammatory genes was also reduced in Rar^{Hom} and Rar^{Het} ILC_{4neg} and LTi_4 cells (Fig. 3a and Extended Data Fig. 4b–d). The marked reduction of *Rorgt* expression suggested that RA could provide ILC_{4neg} cells with signals leading to *Rorgt* regulation. Accordingly, RA stimulation of ILC_{4neg} cells resulted in *Rorgt* upregulation whereas most other transcription factors were unperturbed, notably *Runx1* (Fig. 3b). In agreement, BMS493 inhibited RA-induced *Rorgt* expression, and efficient block of RORγt by digoxin prevented RA-induced differentiation of ILC_{4neg} cells into LTi_4 cells, while cell viability was unaffected (Fig. 3c and Extended Data Fig. 5a–c). To test further whether RA-induced LTi maturation requires RORγt, we determined if differentiation of RAR dominant-negative ILC_{4neg} cells is restored by enforced *Rorgt* expression. Retroviral transduction of *Rorgt* revealed that RAR dominant-negative ILC_{4neg} cells restored high levels of pro-inflammatory genes and reacquired their potential to differentiate towards LTi_4 cells (Fig. 3d–f). Further evidence that RA can directly regulate *Rorgt* expression was provided by computational analysis of potential RARE sites and chromatin immunoprecipitation (ChIP) with pan-RAR and RXR antibodies. RA stimulation resulted in increased binding of RAR and RXR upstream and within the *Rorgt* locus (Fig. 3g, h and Extended Data Table 1). To analyse the role of these sites we introduced the RARE C (−5,478 *Rorg* transcription start site (TSS)), E (−1,800 *Rorg* TSS) and G (−1,619 *Rorgt* TSS) half-sites in a luciferase reporter vector. Mutations in these sites resulted in significant reduction of the regulatory function of these elements as measured by luciferase activity (Fig. 3i). Thus, cell-autonomous RA signalling provides LTi cells with critical differentiation signals via direct regulation of *Rorgt*.

Our data indicate that mature LTi cell numbers regulate the size of SLO primordia and may determine lymphoid organ size in adulthood[24]. Rar^{Het} adult mice had reduced SLOs and lymphocyte numbers when compared to their wild-type littermate controls (Fig. 4a, b and Extended Data Fig. 6a, b). In agreement, mice that received a vitamin-A-deficient (VAD) diet throughout life had reduced lymphoid organ size when compared to vitamin-A-control mice (VAC) (Fig. 4c). However, because Rar^{Het} and VAD lymphocytes are continuously exposed to altered levels of RA signals, it is possible that SLO size might be a consequence of altered lymphocyte pools[12–15]. To clarify this issue, we provided pregnant mice with a vitamin-A-high (VAH), VAD or VAC diet and switched all diets to the same VAC diet after birth. At 10 weeks of age mice that were exposed to a VAH diet exclusively *in utero* had larger SLOs, whereas mice exposed to a VAD diet had small SLOs when compared to VAC control mice (Fig. 4d). Notably, provision of variable vitamin A diet levels exclusively after birth no longer controlled SLO size (Extended Data Fig. 6c, d). Additional evidence that RA determines SLO size in early life was provided by transplantation of CD45.1 wild-type bone marrow into lethally irradiated Rar^{Het} (WT→Rar^{Het}) or wild-type (WT→WT) CD45.2 littermate control hosts at 2 weeks of age (Fig. 4e). Thus, we generated mice that pre- and perinatally received low input of RA signals in haematopoietic cells, but that on transplantation harbour a normal wild-type haematopoietic system. WT→Rar^{Het} mice, which received low RA cues *in utero*, exhibited small SLOs when compared to their WT→WT counterparts at 8 weeks after transplantation (Fig. 4f, g and Extended Data Fig. 6e, f). This phenotype also revealed reduced lymphocyte numbers, albeit normal SLO organization and similar haematopoietic cell reconstitution (Fig. 4h and Extended Data Figs 6f and 7a–d). In agreement, dendritic cells from WT→Rar^{Het} or WT→WT chimaeras had similar capacity to activate lymphocytes (Extended Data Fig. 7e, f).

Our data indicate that available RA *in utero* regulates the size of lymphocyte pools in the offspring, with possible consequences on their adaptive immune responses. To test this hypothesis, WT→Rar^{Het} or WT→WT chimaeras were infected intranasally with murid herpesvirus-4, resulting in acute lung infection. Analysis of draining intrathoracic lymph nodes revealed reduced expansion but normal frequency of $CD8^+$ T cells specific for the viral epitopes ORF61 and ORF75c in WT→Rar^{Het} mice (Fig. 4i and Extended Data Fig. 8a–c). Consequently, whereas

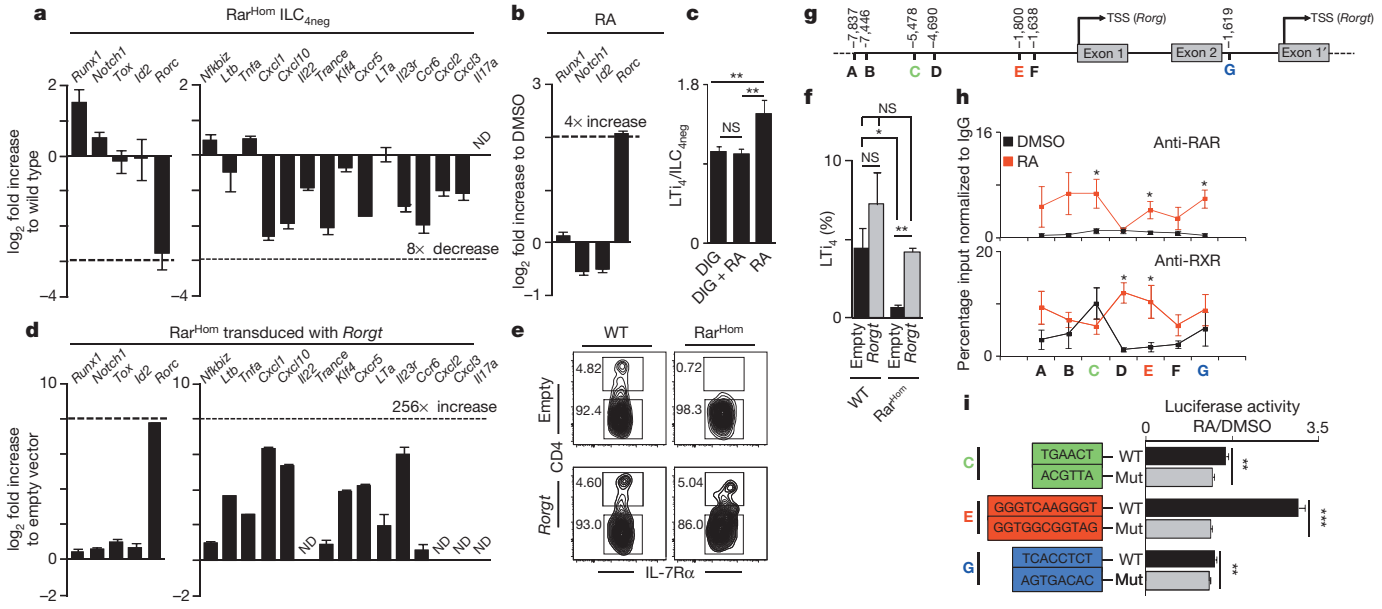

Figure 3 | RA controls LTi cells via RORγt. **a**, E15.5 ILC_{4neg} cells. Data represent three experiments. **b**, E15.5 ILC_{4neg} cells stimulated with RA. Data represent three experiments. **c**, E13.5 lymph node cells stimulated with RA and digoxin (DIG); $n = 16$. **d**–**f**, ILC_{4neg} cells transduced with pMig. *Rorgt*-IRES-GFP virus (day 6). **d**, Data represent three experiments. **e**, Cytometry analysis. **f**, Emergent LTi_4 cells. Wild type (WT), $n = 5$; Rar^{Hom}, $n = 3$. **g**, RARE sites. **h**, E15.5 ILC_{4neg} cells stimulated with RA. ChIP analysis of five biological replicates. **i**, Luciferase activity of RARE wild-type and mutated sites. C, $n = 6$; E, $n = 9$; G, $n = 6$. Error bars show s.e. $^*P < 0.05$; $^{**}P < 0.01$; $^{***}P < 0.001$. NS, not significant. ND, not detected.

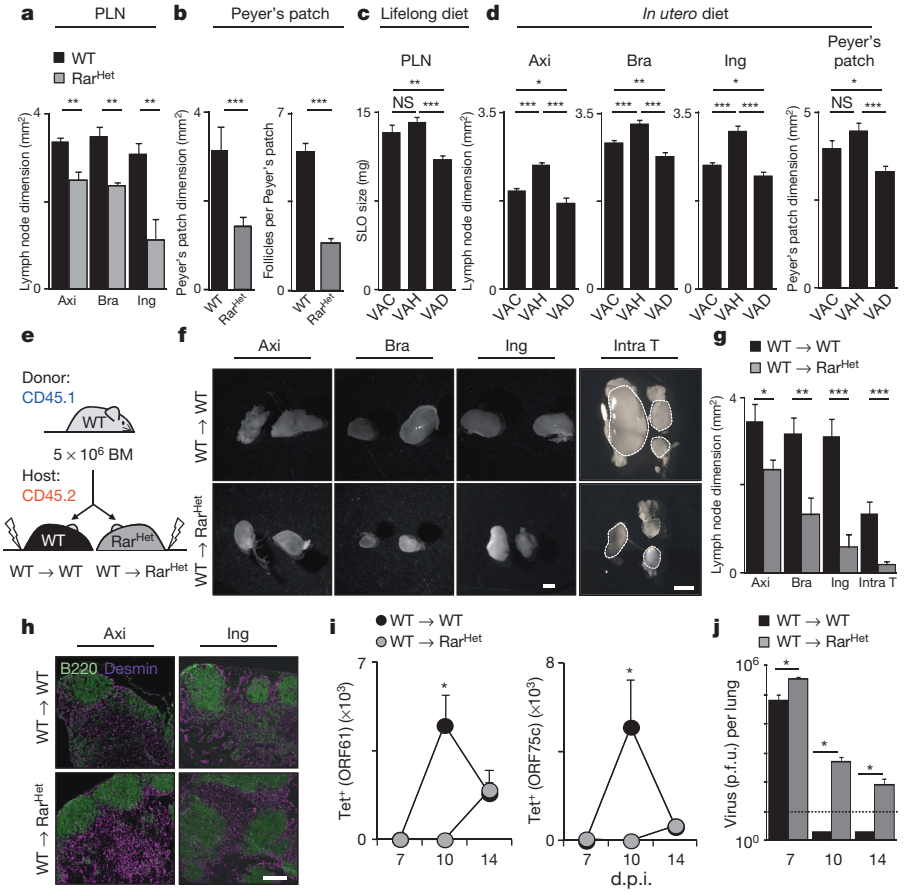

Figure 4 | Retinoid levels *in utero* determine the offspring resistance to infection. **a**, Adult axillary (Axi), brachial (Bra) and inguinal (Ing) peripheral lymph nodes (PLN). $n = 6$. **b**, Peyer's patch area and follicle number per Peyer's patch. Wild type (WT), $n = 26$; Rar^{Het}, $n = 23$. **c**, Females received diets that were maintained in the offspring. VAC, $n = 10$; VAH, $n = 8$; VAD, $n = 18$. **d**, Females received variable diets. Their offspring received VAC diet. Lymph node: VAC, $n = 18$; VAH, $n = 24$; VAD, $n = 25$. Peyer's patch: VAC, $n = 20$; VAH, $n = 40$; VAD, $n = 63$. **e**, Transplantation scheme. **f**, Chimaeric lymph nodes. Scale bar: 1 mm. **g**, Dimensions of chimaeric lymph nodes. $n = 6$. **h**, Chimaeric lymph node structure. Scale bar: 200 μm. **i**, Chimaeras infected with murid herpesvirus-4. Tetramer positive CD8 T cells in intrathoracic lymph nodes. **j**, Virus titres (plaque-forming units (p.f.u.) per lung). 7 days post infection (d.p.i.): WT→WT, $n = 3$; WT→Rar^{Het}, $n = 3$. 10 d.p.i.: WT→WT, $n = 4$; WT→Rar^{Het}, $n = 3$. 14 d.p.i.: WT→WT, $n = 8$; WT→Rar^{Het}, $n = 5$. Dashed line indicates the detection limit. Error bars show s.e. $^{*}P < 0.05$; $^{**}P < 0.01$; $^{***}P < 0.001$. NS, not significant.

WT→WT chimaeras efficiently cleared lytic virus by day 10, high viral titres were still detected in WT→Rar^{Het} chimaeras 14 days after infection (Fig. 4j)[25]. Thus, a deficit of RA signals within haematopoietic cells in early life results in small SLOs and poor capacity to control infection.

Defining the requirements that control SLO development is essential to understand how immunity may be regulated. We now show that RA controls LTi cells, regulating LTi pro-inflammatory genes and the frequency of LTi_4 cells (Extended Data Fig. 9). RA operates in a cell-autonomous fashion, via RORγt, although additional factors regulate *Rorgt* in ILC3s.

SLO development has been considered to be developmentally programmed; we now show that formation of these structures can be also controlled by dietary signals. Thus, in addition to the established impact of dietary plant-derived chemicals in postnatal immune cells, our work reveals dietary retinoids as key regulators of pre-natal ILCs with a lifelong impact on adult lymphoid organ size[26–28]. It was previously shown that complete absence of lymphoid organs leads to long-life virus persistence[29]. Our data reveal that the efficiency of adaptive immune responses to infection and possibly to other immune insults may be pre-tuned in early life through dietary signals from maternal origin.

We report here that cell-autonomous RA signalling is a key axis for *Rorgt* expression and LTi cell differentiation within developing SLOs. Similarly, RA may also be important after birth in infection and chronic inflammatory diseases[30]. Lineage-targeted strategies will be central to elucidate the contribution of dietary retinoids in these outcomes.

METHODS SUMMARY

Mice were maintained at Instituto de Medicina Molecular (IMM) or VU University Medical Centre according to national and international guidelines. Bone marrow cells were isolated from 8-week-old C57BL/6 CD45.1 mice and injected intravenously into 2-week-old lethally irradiated CD45.2 *ROSA26*-RARα403^{Het} (WT→Rar^{Het}) or wild-type littermate controls (WT→WT). C57BL/6 female mice received either vitamin-A-deficient (VAD), with no vitamin A (vitamin free casein), vitamin-A-high (VAH, 25,000 IU kg^{-1}) or vitamin-A-control (VAC, 4,000 IU kg^{-1}) diets. Retinoic acid was provided to pregnant mice from E10.5 until they were euthanized. Quantitative real-time PCR with reverse transcription (RT–PCR) was performed as previously described[6,7,10]. Computational analysis was performed with TESS. DNA–protein complexes were immunoprecipitated using antibodies against mouse pan-RAR, pan-RXR or control IgG.

Online Content Any additional Methods, Extended Data display items and Source Data are available in the online version of the paper; references unique to these sections appear only in the online paper.

Received 6 June 2013; accepted 18 February 2014.
Published online 19 March 2014.

1. Gluckman, P. D. & Hanson, M. A. Living with the past: evolution, development, and patterns of disease. *Science* **305,** 1733–1736 (2004).
2. van de Pavert, S. A. & Mebius, R. E. New insights into the development of lymphoid tissues. *Nature Rev. Immunol.* **10,** 664–674 (2010).
3. Randall, T. D., Carragher, D. M. & Rangel-Moreno, J. Development of secondary lymphoid organs. *Annu. Rev. Immunol.* **26,** 627–650 (2008).
4. Mebius, R. E., Rennert, P. & Weissman, I. L. Developing lymph nodes collect $CD4^{+}CD3^{-}LT\beta^{+}$ cells that can differentiate to APC, NK cells, and follicular cells but not T or B cells. *Immunity* **7,** 493–504 (1997).

5. Eberl, G. *et al.* An essential function for the nuclear receptor RORγt in the generation of fetal lymphoid tissue inducer cells. *Nature Immunol.* **5,** 64–73 (2004).
6. Veiga-Fernandes, H. *et al.* Tyrosine kinase receptor RET is a key regulator of Peyer's Patch organogenesis. *Nature* **446,** 547–551 (2007).
7. Patel, A. *et al.* Differential RET signaling pathways drive development of the enteric lymphoid and nervous systems. *Sci. Signal.* **5,** ra55 (2012).
8. Cupedo, T. *et al.* Presumptive lymph node organizers are differentially represented in developing mesenteric and peripheral nodes. *J. Immunol.* **173,** 2968–2975 (2004).
9. Cherrier, M., Sawa, S. & Eberl, G. Notch, Id2, and RORγt sequentially orchestrate the fetal development of lymphoid tissue inducer cells. *J. Exp. Med.* **209,** 729–740 (2012).
10. van de Pavert, S. A. *et al.* Chemokine CXCL13 is essential for lymph node initiation and is induced by retinoic acid and neuronal stimulation. *Nature Immunol.* **10,** 1193–1199 (2009).
11. Niederreither, K. & Dolle, P. Retinoic acid in development: towards an integrated view. *Nature Rev. Genet.* **9,** 541–553 (2008).
12. Iwata, M. Retinoic acid production by intestinal dendritic cells and its role in T-cell trafficking. *Semin. Immunol.* **21,** 8–13 (2009).
13. Hall, J. A. *et al.* Essential role for retinoic acid in the promotion of $CD4^+$ T cell effector responses via retinoic acid receptor alpha. *Immunity* **34,** 435–447 (2011).
14. Mora, J. R. & von Andrian, U. H. Role of retinoic acid in the imprinting of gut-homing IgA-secreting cells. *Semin. Immunol.* **21,** 28–35 (2009).
15. Mucida, D. *et al.* Retinoic acid can directly promote TGF-β-mediated $Foxp3^+$ Treg cell conversion of naive T cells. *Immunity* **30,** 471–472; Reply 472–473 (2009).
16. Hall, J. A., Grainger, J. R., Spencer, S. P. & Belkaid, Y. The role of retinoic acid in tolerance and immunity. *Immunity* **35,** 13–22 (2011).
17. de Boer, J. *et al.* Transgenic mice with hematopoietic and lymphoid specific expression of Cre. *Eur. J. Immunol.* **33,** 314–325 (2003).
18. Rosselot, C. *et al.* Non-cell-autonomous retinoid signaling is crucial for renal development. *Development* **137,** 283–292 (2010).
19. Sun, Z. *et al.* Requirement for RORγ in thymocyte survival and lymphoid organ development. *Science* **288,** 2369–2373 (2000).
20. Yokota, Y. *et al.* Development of peripheral lymphoid organs and natural killer cells depends on the helix-loop-helix inhibitor Id2. *Nature* **397,** 702–706 (1999).
21. Aliahmad, P., de la Torre, B. & Kaye, J. Shared dependence on the DNA-binding factor TOX for the development of lymphoid tissue-inducer cell and NK cell lineages. *Nature Immunol.* **11,** 945–952 (2010).
22. Possot, C. *et al.* Notch signaling is necessary for adult, but not fetal, development of $ROR\gamma t^+$ innate lymphoid cells. *Nature Immunol.* **12,** 949–958 (2011).
23. Tachibana, M. *et al.* Runx1/Cbfβ2 complexes are required for lymphoid tissue inducer cell differentiation at two developmental stages. *J. Immunol.* **186,** 1450–1457 (2011).
24. Meier, D. *et al.* Ectopic lymphoid-organ development occurs through interleukin 7-mediated enhanced survival of lymphoid-tissue-inducer cells. *Immunity* **26,** 643–654 (2007).
25. Gredmark-Russ, S., Cheung, E. J., Isaacson, M. K., Ploegh, H. L. & Grotenbreg, G. M. The CD8 T-cell response against murine gammaherpesvirus 68 is directed toward a broad repertoire of epitopes from both early and late antigens. *J. Virol.* **82,** 12205–12212 (2008).
26. Kiss, E. A. *et al.* Natural aryl hydrocarbon receptor ligands control organogenesis of intestinal lymphoid follicles. *Science* **334,** 1561–1565 (2011).
27. Lee, J. S. *et al.* AHR drives the development of gut ILC22 cells and postnatal lymphoid tissues via pathways dependent on and independent of Notch. *Nature Immunol.* **13,** 144–151 (2011).
28. Qiu, J. *et al.* The aryl hydrocarbon receptor regulates gut immunity through modulation of innate lymphoid cells. *Immunity* **36,** 92–104 (2011).
29. Karrer, U. *et al.* On the key role of secondary lymphoid organs in antiviral immune responses studied in alymphoplastic (*aly/aly*) and spleenless (*Hox11*$^{-/-}$) mutant mice. *J. Exp. Med.* **185,** 2157–2170 (1997).
30. Spencer, S. P. *et al.* Adaptation of innate lymphoid cells to a micronutrient deficiency promotes type 2 barrier immunity. *Science* **343,** 432–437 (2014).

Acknowledgements We thank the imaging, animal and flow cytometry facilities at IMM and UPC for technical assistance; C. Mendelsohn for providing *ROSA26*-RARα403 mice; N. Schmolka, J. G. van Rietschoten, R. E. van Kesteren, T. H. B. Geijtenbeek, S. Gringhuis, E. Keuning, J. Peterson-Maduro, M. G. Roukens, D. D'Astolfo, M. Vermunt, A. Rijerkerk, J. Koning, J. van der Meulen and B. Oliver for technical help; and G. Vilhais-Neto, M. C. Coles and G. Eberl for discussion. M.F., L.M.-S. and R.G.D. were supported by FCT, Portugal; H.V.-F. by EMBO (1648) and ERC (207057); D.R.L. by NIH (RO1AI080885) and HHMI; M.R.M. by Dutch MS research foundation (MS 12-797); S.A.vd.P. by NGI Breakthrough Horizon (40-41009-98-9077); and R.E.M. by a VICI (918.56.612) and ALW-TOP grant (09.048).

Author Contributions M.F. wrote the manuscript, designed, performed and analysed the experiments in Figs 1a, b, d, e, g–i, 2a–h, 3a, b, d–i and 4a, b, d–j and Extended Data Figs 1a, d–f, 2a–d, 3a–h, 4a–d, 5a–c, 6, 7a–f, 8a–d, 9a, b and 10a–c. S.A.vd.P. wrote the manuscript, designed, performed and analysed the experiments in Figs 1c, f, 3c, g–i and 4c and Extended Data Figs 1b, c, e, 5b, c and 6. R.G.D., H.R., R.M., L.M.-S., F.F.A., S.I., I.B., G.G., C.L.-A., T.K., D.S., T.O'T., M.R.M., Y.H. and S.S-M. contributed to several experiments. C.G.-S. and J.P.S. provided murid herpesvirus-4. D.R.L. and F.R.S provided *Rorgt*$^{-/-}$ embryos. E.H. and E.D. provided Ly-6A (*Sca1*)-*GFP* mice. R.E.M. and H.V.-F. supervised the work, planned the experiments and wrote the manuscript.

Author Information Reprints and permissions information is available at www.nature.com/reprints. The authors declare no competing financial interests. Readers are welcome to comment on the online version of the paper. Correspondence and requests for materials should be addressed to H.V.-F. (jhfernandes@medicina.ulisboa.pt).

METHODS

Mice. C57BL/6 mice were purchased from Charles River and C57BL/6 CD45.1 mice were obtained at IMM. *Vav-iCre* (ref. 17), *hCD2-GFP* (ref. 6), *Id2-CreERT2* (ref. 31), *ROSA26-RARα403* (ref. 18), *Rorgt-Cre* (ref. 32), *ROSA26-eYFP* (ref. 33), *hCD2-Cre* (ref. 17), *ROSA26-mGFPTomato* (ref. 34), Ly-6A (*Sca1*) *GFP* (ref. 35), $Rorgt^{-/-}$ (ref. 19), *Id2-GFP* (ref. 31), and *OT1* Tg $Rag1^{-/-}$ (refs 36, 37) mice were previously described. Tamoxifen (2 mg per female) was injected daily into *Id2-creERT2* pregnant females from E8.5 to E13.5. All animal experiments were approved by national and institutional ethical committees: Direção Geral de Veterinária and Instituto de Medicina Molecular (IMM) ethical committee and Animal Experimental Committee, VU University (VUMC). Power analysis was performed to estimate the number of experimental mice.

Bone marrow transplantation. Bone marrow cells were isolated from 8-week-old C57BL/6 CD45.1 mice and 5×10^6 cells were injected intravenously into 2-week-old lethally irradiated (1,000rad) CD45.2 *ROSA26*-RARα403^{Het} (WT→Rar^{Het}) or CD45.2 wild-type littermate controls (WT→WT).

Vitamin A diets. C57BL/6 female mice received either vitamin-A-deficient (VAD), with no vitamin A (vitamin free casein), vitamin-A-high (VAH, 25,000 IU kg^{-1}) or vitamin-A-control (VAC, 4,000 IU kg^{-1}) diet at E8.5 or 2 weeks before coitus in Fig. 4d. Diets were purchased from MP Biomedical (AIN93M feed, Solon) (see below). RA is rapidly degraded under normal light and temperature conditions; thus it is unlikely that bioactive RA is present in normal diets. Therefore, bioactive RA levels in the differently used diets or normal chow is negligible. Analysis of the adult offspring with lifelong diet (mice kept under VAD, VAH or VAC diet until analysis) was performed at 10 weeks of age. Analysis of the adult offspring with pre- and perinatal VAH and VAD diet (*in utero*) was performed at 10 weeks of age (all mice were switched to the same VAC diet after birth). Post-birth diet experiments (VAD, VAH and VAC) were initiated at 6 weeks of age and analysed at 13 weeks of age. For adult SLO analysis axillary, brachial, inguinal and intrathoracic lymph nodes and Peyer's patches were carefully dissected. Dimensions were determined using a Zeiss Stereo Lumar V12 microscope with a Zeiss Neolumar S 0.8X objective and weights determined with precision scales (Sartorius). The vitamin-A-deficient diet had similar composition to the control diet but with no added vitamin A palmitate. Vitamin-A-high diet contained 1 g vitamin A palmitate (250,000 U g^{-1}) per 10 kg of diet. Thus, 10 kg of vitamin-A-control diet was composed of 4,657 g corn starch, 1,400 g vitamin free casein, 1,550 g dextrinized corn starch, 1,000 g sucrose, 400 g soybean oil, 500 g Alphacel non-nutritive bulk, 350 g AIN-93M mineral mix, 108 g L-cystine, 25 g choline bitartrate, 0.080 g T-butyl hydroquinone, 0.3 g niacin, 0.16 g D-calcium pantothenate, 0.07 g pyridoxine HCl, 0.06 g thiamine HCl, 0.06 g riboflavin, 0.02 g folic acid, 0.002 g biotin, 0.25 g vitamin B-12 (0.1% Trit), 3 g alpha tocopherol powder (250 U g^{-1}), 0.16 g vitamin A palmitate (250,000 U g^{-1}), 0.025 g vitamin D3 (400,000 U g^{-1}), 0.008 g phylloquinone and 96 g powder sugar.

Retinoic acid and BMS493 treatment. For *in vivo* stimulation, retinoic acid was provided to pregnant mice as previously described[38]. In short, mice were mated overnight and the day of vaginal plug detection was marked as E0.5. Retinoic acid supplemented food was given from E10.5 until death (Sigma-Aldrich, 250 mg g^{-1} chow or vehicle, that is, ethanol). Food was stored in the dark at 4 °C and refreshed every day until death. For *in vivo* blocking of retinoic acid signalling, pregnant C57BL/6 mice were treated with pan-RAR inverse agonist BMS493 (Tocris Bioscience) (5 mg kg^{-1}) or vehicle (DMSO) 1:10 in corn oil.

Kidney capsule and *ex-vivo* differentiation assay. E12.5 intestines (CD45.2) were transplanted under the kidney capsule of anaesthetized 6–7-week-old C57BL/6 CD45.1 mice. For explant organ cultures E12.5 intestines were micro-dissected and cultured as previously described[6,39]. Intestines were digested with collagenase D (5 mg ml^{-1}; Roche) and DNase I (0.1 mg ml^{-1}; Roche) and were analysed by flow cytometry.

Confocal microscopy. Gut whole-mount analysis was performed as previously described[6,39]. For embryo whole-mount analysis, E15.5 mice were fixed with 4% paraformaldehyde and incubated in blocking/permeabilizing buffer (PBS containing 10% fetal bovine serum, 2% BSA and 0.3% Triton X-100). Embryos were incubated at 4 °C overnight with primary and secondary antibodies. Samples were cleared using benzyl-alcohol-benzyl-benzoate (BABB) and were imaged in a Zeiss LSM 710 (Carl Zeiss) using EC Plan-Neofluar 10×/0.30 M27 and objective Plan Apochromat 20x/0.8 M27. Images were processed using Zeiss LSM Image Browser 4.2 software (Carl Zeiss).

Immunofluorescence analysis of embryo sections was performed as previously described[10]. Briefly, samples were formalin-fixed and 8 μm cryosections were dehydrated in acetone for 10 min. Sections were air-dried for 10 min. Cryosections were post-fixed 30 min with 1% formalin, pre-incubated for 1 h with PBS containing 10% normal goat serum and 0.2% Triton X-100. Sections were incubated 90 min with primary and secondary antibodies in PBS containing 0.2% Triton X-100 and 2% normal goat serum. Sections were embedded in Mowiol with DAPI (Calbiochem) and analysed using Leica SP2 confocal laser scanning microscope.

For immunofluorescence analysis of adult lymph nodes, samples were snap frozen in isopenthane pre-cooled in liquid nitrogen and kept at −80 °C. Lymph nodes were sectioned (5 μm sections), fixed with 4% paraformaldehyde for 10 min and incubated in blocking/permeabilizing buffer (PBS containing 10% fetal bovine serum, 2% BSA and 0.3% Triton X-100). Samples were incubated with primary and secondary antibodies overnight or for 2 h in PBS containing 10% fetal bovine serum, 2% BSA and 0.3% Triton X-100. Sections were mounted in Mowiol with DAPI (Calbiochem). Images were acquired on Zeiss LSM 710 (Carl Zeiss) using EC Plan-Neofluar 10×/0.30 M27 and objective Plan Apochromat 20×/0.8 M27. Images were processed using Zeiss LSM Image Browser 4.2 software (Carl Zeiss).

Flow cytometry analysis and cell sorting. Embryonic guts and lymph nodes were collected, digested with collagenase D (5 mg ml^{-1}; Roche) or Blenzyme 2 (0.5 mg ml^{-1}, Roche) and DNase I (0.1 mg ml^{-1}; Roche) in DMEM, 3% FBS for approximately 40 min at 37 °C under gentle agitation. Fetal liver, adult spleen and lymph node cell suspensions were obtained using 70 μm strainers. Lineage (Lin) was: Ter119, TCRβ, CD3ε, CD19, NK1.1, CD11c and Gr1. Flow cytometry analysis and cell sorting were performed using FORTESSA, FACSCanto I, FACSAria I and II flow cytometers (BD Biosciences), MoFlo XDP or Cyan ADP flow cytometer (Beckman Coulter). Data analysis was done using FlowJo software (Tristar). Sorted populations were >95% pure.

Cell culture and viral transduction. For *in vitro* stimulation, lymph node embryonic cells were collected as previously described[10]. Tissues were digested with Blenzyme 2 (0.5 mg ml^{-1}, Roche), DNaseI (0.2 mg ml^{-1}, Roche) in PBS for 15 min at 37 °C while stirring constantly. Cell suspensions were washed with RPMI (Invitrogen), supplemented with 2% heat-inactivated FCS, 100 U ml^{-1} penicillin, and 100 μg ml^{-1} streptomycin. For retinoic acid stimulation experiments, *all-trans* retinoic acid (Sigma-Aldrich) dissolved at 10 mM in 100% ethanol was added at 100 nM as previously described[10]. After 24 h incubation at 37 °C and 5% CO_2, cells were isolated and analysed by flow cytometry and RT–PCR. Efficiency of RA treatment was assessed by expression of the RA target gene *Rarb* (ref. 16).

Digoxin (Sigma-Aldrich) was dissolved in ethanol at 10 mM and used at 10 μM, as previously described[40]. Efficiency of digoxin treatment was assessed by expression of the RORγt target genes *Il1r1*, *Il17a*, *Il23r*, *Ccr6*, *Ccl20* and *Csf2* (ref. 40).

For treatment of ILC_{4neg} cells *in vitro*, guts and lymph nodes from E15.5 embryos were collected, digested with collagenase D (5 mg ml^{-1}; Roche) and DNaseI (0.1 mg ml^{-1}; Roche) in DMEM, 3% FBS, for approximately 40 min at 37 °C with gentle agitation. Total cell suspension or flow cytometry sorted cells were starved overnight and stimulated with *all-trans* retinoic acid (Sigma-Aldrich, 1 μM) or vehicle (DMSO, 0.0015%, Sigma-Aldrich) for 24 h at 37 °C and 5% CO_2. Cells were analysed by flow cytometry or quantitative real-time RT–PCR. For cell culture, ILC_{4neg} cells were sorted from E15.5 guts and lymph nodes and suspended in culture medium OPTI MEM (Invitrogen) supplemented with 20% FBS, penicillin and streptomycin (respectively 50 U and 50 mg ml^{-1}, Invitrogen), sodium pyruvate (1 mM, Invitrogen) and β-mercaptoethanol (50 mM, Invitrogen) and recombinant murine RANK ligand (rRANKL; 50 ng ml^{-1}; Peprotech). Cells were seeded into flat-bottom 96-well plates previously coated with 3,000-rad-irradiated OP9 stromal cells for 6 days. E15.5 ILC_{4neg} cells from RAR dominant-negative and wild-type littermate controls were sorted and transduced with pMig.IRES-GFP retroviral empty vector or containing *Rorgt* in the presence of polybrene (0.8 mg ml^{-1}; Sigma-Aldrich). pMig.IRES-*Rorgt* was a gift from D. R. Littman (Addgene plasmid no. 24069). Transduced cells were cultured for 6 days. Cultured cells were trypsinized and directly analysed by flow cytometry or FACS sorted and analysed by RT–PCR.

Quantitative RT–PCR. Total RNA was extracted using RNeasy micro kit (Qiagen) or using Trizol (Invitrogen) according to the manufacturer's protocol. RNA concentration was determined using Nanodrop Spectrophotometer (Nanodrop Technologies). Quantitative real-time RT–PCR was performed as previously described[6,7,10]. Listed primers are sense and antisense, respectively. When a nested-sense primer was used, this is last in the list. Gene sequences were obtained from http://www.ensembl.org. *Rara* 5′-GCATCCAGAAGAACATGGTG-3′ and 5′-CTCGTTGTTCTGAGCTGTTG-3′; *Rarb* 5′-AGCCCACCATCTCCACTTC-3′ and 5′-CTCGATGGCAAGTGTAGATC-3′; *Rarg* 5′-TGCAATGACAAGTCTTCTGG-3′ and 5′-GTTTTTGTCACGGTGACATG-3′; *Rxra* 5′-TTCTCTACCCAGGTGAACTC-3′ and 5′-AGGAGGCCATATTTCCTGAG-3′; *Rxrb* 5′-CAAAGACTGTACAGTGGAC-3′ and 5′-CCTTGGTCACTCTTCTGCTC-3′; *Rxrg* 5′-TCTTGGCTCTCCGTATAGAG-3′ and 5′-CTGCTGACACTGTTGACCAC-3′; *Hprt1* 5′-TCCCTGGTTAAGCAGTACAG-3′, 5′-GCTTTGTATTTGGCTTTTCC-3′ and 5′-GACCTCTCGAAGTGTTGGAT-3′.

TaqMan specific primers and probes were from Applied Biosystems. TaqMan Gene Expression Assays were the following: *Gapdh* Mm99999915_g1; *Hprt1* Mm00446968_m1; *Id2* Mm00711781_m1; *Runx1* Mm01213405_m1; *Lta* Mm00440228_gH; *Trance* Mm00441906_m1; *Cxcl10* Mm00445235_m1; *Cxcr5* Mm00432086_m1; *Ccr6* Mm99999114_s1; *Cxcl3* Mm01701838_m1; *Tnfa* Mm00443260_g1; *Cxcl1* Mm04207460_m1; *Nfkbiz* Mm00600522_m1; *Cxcl2* Mm00436450_m1; *Klf4*

Mm00516104_m1; *Tox* Mm00455231_m1; *Il22* Mm01226722_g1; *Il17a* Mm00439618_m1; *Il23r* Mm00519943_m1; *Rorc* Mm01261022_m1; *Ltb* Mm00434774_g1; *Notch1* Mm00435249_m1; *Il1r1* Mm00434237_m1; *Ccl20* Mm01268754_m1; and *Csf2* Mm01290062_m1. Gene expression was normalized to *Hprt1* and *Gapdh*. Real-time PCR analysis was performed using ABI Prism 7900HT Sequence Detection System or StepOne Real-Time PCR system (Applied Biosystems).

Bioinformatics and chromatin immunoprecipitation (ChIP) assay. TESS (http://www.cbil.upenn.edu/tess) web-based tool was used to identify putative RA response elements (RARE) in the mouse *Rorc* locus. Embryonic ILC_{4neg} cells (2×10^5) were isolated by flow cytometry from E15.5 intestines and PLNs. Cell suspensions were starved overnight and incubated with *all-trans* RA (1 μM) or DMSO (0.0015%) for 8 h and fixed with 0.8% formaldehyde (EMS sciences). Cells were lysed and chromosomal DNA–protein complex sonicated to generate DNA fragments ranging from 100 to 300 bp. DNA–protein complexes were immunoprecipitated using 6 μg of rabbit polyclonal antibody against mouse pan-RAR (M-454, Santa Cruz Biotech, Inc.), 4 μg of rabbit polyclonal antibody against mouse pan-RXR (ΔN197, Santa Cruz Biotech, Inc.) or rabbit control IgG (Abcam). Immunoprecipitates were uncrosslinked and analysed by quantitative PCR using primer pairs flanking putative RARE sites: A, F-TGAAGCAGCTAGTCACTTCC and R-CAGCTCTCCAGCTTGTATTG; B, F-GAAACTTTATCTGGGGCTGG and R-TGAACTCAGGAAGAGCAGCA; C, F-AACCTGGCACTTCGCACTTAA and R-GAGTGGGCGGACTTCTCAGA; D, F-GAGGCCTCTAAGTACCGCCATT and R-CGCCCTGAATCCTGTCACA; E, F-CAGAGATGACCTAGTCAGTGG AGTACTG and R-ACCCCCCAAAACCCTTGA; F, F-ACCACTGAGCCATCT CTCCTACC and R-TTTTGTGATGTGGGTTCTGGG; G, F-GACAATCTCAT CAGAGGAGG and R-GGGCAACCAATGAGTATGTG. Results were normalized to input, intensity and control IgG.

Luciferase reporter assay. Putative RARE sequences were cloned into pTA-Luc firefly Luciferase reporter plasmid (Clontech). Corresponding scrambled mutated sequences were also cloned into the same plasmid. Sequences were cloned in tandems (four copies). Wild-type and scrambled sequences (1 copy) were, respectively: C: AACCTGGCACTTCGCACTTAAACCTGTGAACTCTGAGAAGTCCGCC CACTC and AACCTGGCACTTCGCACTTAAACCTGACGTTACTGAGAAG TCCGCCCACTCE; E: CAGAGATGACCTAGTCAGTGGAGTACTGCCACA AACACACTGGGGTCAAGGGTTTTGGGGGGT and CAGAGACACTTGAGT CAGTGGAGTACTGCCACAAACACACTAGGTGGCGGTAGTTTGGGGGGT; G: GACAATCTCATCAGAGGAGGTCACCTCTACTCTTCCATCACATACTC ATTGGTTGCCC and GACAATCTCATCAGAGGCCTAGTGACACTCTCTT CCATCACATACTCATTGGTTGCCC. Putative binding sites and respective scrambled sequences are underlined. To test the activity of these elements, 293T cells were transfected with the aforementioned reporter constructs together with expression vectors expressing murine RARα, RXRα (gift from G. C. Vilhais-Neto and O. Pourquié) and *Renilla*-Luciferase using X-tremeGene9 DNA Transfection Reagent (Roche). At 48 h cells were starved and 20 h later treated with DMSO or RA (1 μM) for 24 h, and Luciferase activity was measured in total cell lysates using the Dual-Luciferase Reporter Assay System (Promega). Data were normalized for transfection efficiency using the ratio between firefly Luciferase activity and *Renilla* Luciferase.

Murid herpesvirus-4 infection. Chimaeric mice obtained from transplantation of wild-type bone marrow (CD45.1) into lethally irradiated Rar^{Het} (WT→Rar^{Het}) or wild-type (WT→WT) littermate control hosts (CD45.2) were used. Mice were infected intranasally with 10^4 p.f.u. of murid herpesvirus-4 (MuHV-4)[41,42] under isofluorane anaesthesia 12 weeks after transplantation. Intrathoracic lymph nodes and lungs were removed for analysis. Titres of lytic (infectious) virus were determined by plaque assay of freeze-thawed lung tissue homogenates on BHK-21 cells. Plates were incubated for 4 days, then fixed with 4% formal saline and counterstained with toluidine blue for plaque counting. Frequency and number of virus-specific CD8 T cells (Tetramer positive) for two viral epitopes (ORF61 and ORF75c) were determined in the draining intrathoracic lymph nodes by tetramer staining (a gift from H. L. Ploegh) and flow cytometry[25].

OT1 CD8 T-cell activation. Dendritic cells were isolated from single-cell suspensions of lymph nodes and spleen from WT→Rar^{Het} or WT→WT chimaeric mice. Cells were negatively depleted for TCRβ, CD19, TER119, Mac1, Gr1, CD3ε using DynaBeads Biotin Binder kit (Life Technologies) and positively enriched for CD11c using MACS Cell Separation Reagents (Miltenyi Biotech). OT1 CD8 T cells were isolated from peripheral lymph nodes of OT1 Tg *Rag1*$^{-/-}$ mice by Thy1.2 positive enrichment using MACS Cell Separation Reagents (Miltenyi Biotech). 2.5×10^4 dendritic cells pre-loaded with 10^{-5} μM OVA peptide (Thermo Scientific) were cultured for 3 days with 1.25×10^5 monoclonal OT1 CD8 T cells labelled with 2 μM CFSE (BioLegend). Expansion of OT1 CD8 T cells was measured by CFSE dilution and proliferative index was calculated using FlowJo (TreeStar, Inc.). Intracellular IFN-γ levels were measured by flow cytometry using IC fixation/permeabilization kit (eBioscience).

Antibody list. Cell suspensions were stained for flow cytometry using: anti-CD45 (30-F11); anti-CD11c (N418); anti-CD127 (IL-7Rα; A7R34); anti-Ly-6A/E (Sca1; D7); anti-CD45.1 (A20); anti-CD45.2 (104); anti-CD8α (53-6.7); anti-CD19 (eBio1D3); anti-Thy1.2 (53-2.1); anti-NK1.1 (PK136); anti-CD3ε (eBio500A2), anti-TER119 (TER-119), anti-CD11b (Mi/70), anti-Gr1 (RB6-8C5), anti-IFN-γ (XMG1.2), isotype for IFN-γ (eBRG1), anti-α4β7 (DATK32) and anti-MHCII (M5/114.15.2) antibodies and streptavidin fluorochrome conjugates from eBioscience. Anti-CD4 (GK1.5) and TCRβ (H57-595) antibodies were purchased from Biolegend. Anti-RORγt (Q31-378) and RORγt isotype (G155-178) were purchased from BD Pharmingen. Anti-GFP (A11008) antibody was purchased from Invitrogen. Intracellular staining for flow cytometry was performed using IC fixation/permeabilization kit (eBioscience). Embryo sections for immunofluorescence analysis were stained with GK1.5 (anti-CD4), MP33 (anti-CD45) and A7R34 (anti-IL-7Rα; provided by S. Nishikawa) purified from hybridoma cell culture supernatants with protein G-Sepharose (Pharmacia). Anti-Ki67 and anti-podoplanin (8.1.1) antibodies were purchased from BD Biosciences and Biolegend, respectively. Embryos were whole-mount-stained using Alexa Fluor 647-conjugated anti-CD4 (YTS191.1) from AbDSerotec; intestines were whole-mount-stained using rat anti-CD106 (VCAM-1, 429 MVCAM.A) from BD Biosciences. Adult lymph node sections were stained using rabbit polyclonal anti-desmin and rat monoclonal anti-B220 (RA3-6B2) from Abcam and eBioscience, respectively. Anti-species-specific Alexa Fluor 594, Alexa Fluor 555, Alexa Fluor 488 or Alexa Fluor 647 were used as secondary antibodies (Invitrogen).

Statistics. Variance was analysed using an *F*-test. Student's *t*-test was performed on homoscedastic populations and Student's *t*-test with Welch correction was applied on samples with different variances.

31. Rawlins, E. L., Clark, C. P., Xue, Y. & Hogan, B. L. The $Id2^+$ distal tip lung epithelium contains individual multipotent embryonic progenitor cells. *Development* **136,** 3741–3745 (2009).
32. Eberl, G. & Littman, D. R. Thymic origin of intestinal αβ T cells revealed by fate mapping of RORγt$^+$ cells. *Science* **305,** 248–251 (2004).
33. Srinivas, S. *et al.* Cre reporter strains produced by targeted insertion of EYFP and ECFP into the ROSA26 locus. *BMC Dev. Biol.* **1,** 4 (2001).
34. Muzumdar, M. D., Tasic, B., Miyamichi, K., Li, L. & Luo, L. A global double-fluorescent Cre reporter mouse. *Genesis* **45,** 593–605 (2007).
35. de Bruijn, M. F. *et al.* Hematopoietic stem cells localize to the endothelial cell layer in the midgestation mouse aorta. *Immunity* **16,** 673–683 (2002).
36. Hogquist, K. A. *et al.* T cell receptor antagonist peptides induce positive selection. *Cell* **76,** 17–27 (1994).
37. Mombaerts, P. *et al.* RAG-1-deficient mice have no mature B and T lymphocytes. *Cell* **68,** 869–877 (1992).
38. Niederreither, K. *et al.* Embryonic retinoic acid synthesis is essential for heart morphogenesis in the mouse. *Development* **128,** 1019–1031 (2001).
39. Veiga-Fernandes, H., Foster, K., Patel, A., Coles, M. & Kioussis, D. Visualisation of lymphoid organ development. *Methods Mol. Biol.* **616,** 161–179 (2010).
40. Huh, J. R. *et al.* Digoxin and its derivatives suppress TH17 cell differentiation by antagonizing RORγt activity. *Nature* **472,** 486–490 (2011).
41. Sunil-Chandra, N. P., Efstathiou, S., Arno, J. & Nash, A. A. Virological and pathological features of mice infected with murine gamma-herpesvirus 68. *J. Gen. Virol.* **73,** 2347–2356 (1992).
42. Weck, K. E., Barkon, M. L., Yoo, L. I., Speck, S. H. & Virgin, H. I. Mature B cells are required for acute splenic infection, but not for establishment of latency, by murine gammaherpesvirus 68. *J. Virol.* **70,** 6775–6780 (1996).

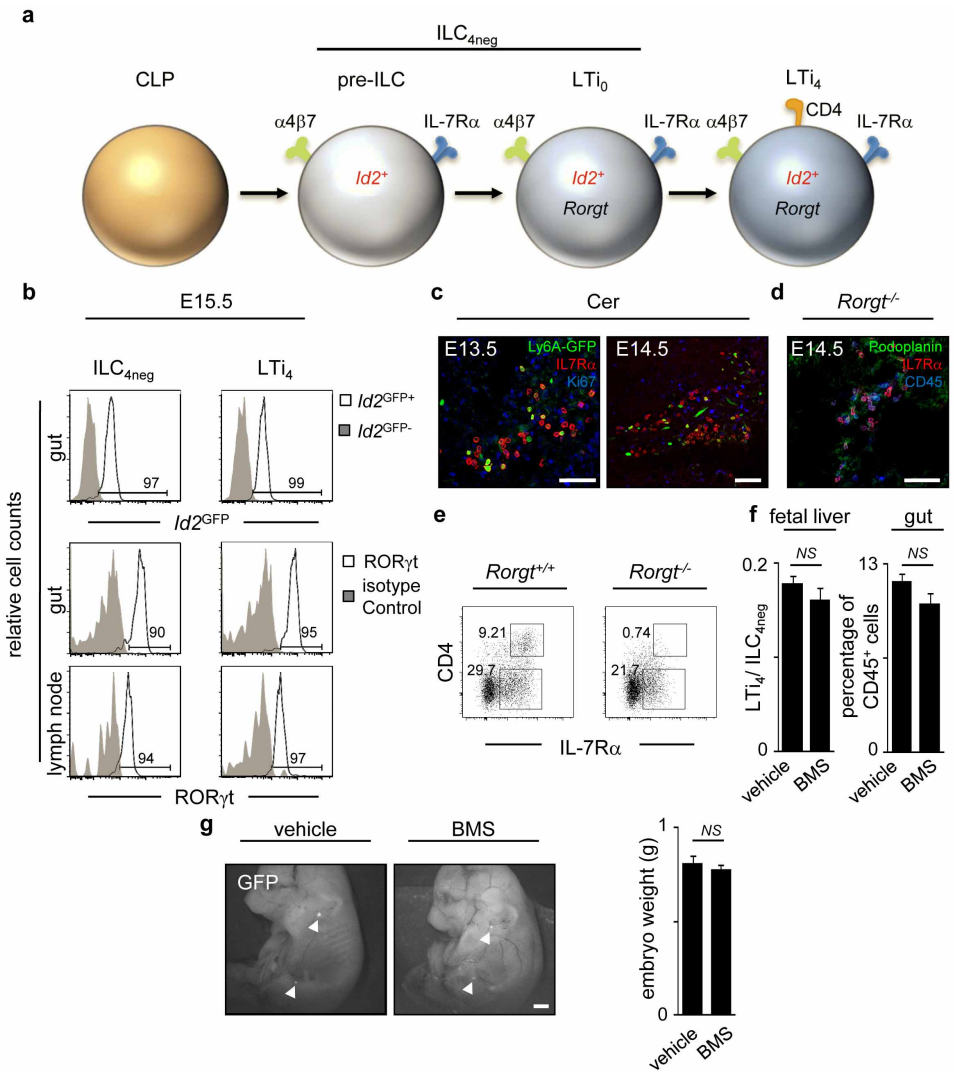

Extended Data Figure 1 | Fetal ILCs. **a**, ILC subsets in fetal gut and lymph nodes (LNs). **b**, E15.5 intestines and lymph node cells were purified from *Id2*^{GFP} and wild-type mice. *Id2*^{GFP} and RORγt expression are shown in ILC_{4neg} ($CD3^-IL\text{-}7R\alpha^+\alpha4\beta7^+ID2^+c\text{-}Kit^+CD11c^-CD4^-$) and LTi_4 ($CD3^-IL\text{-}7R\alpha^+\alpha4\beta7^+ID2^+c\text{-}Kit^+CD11c^-ROR\gamma t^+CD4^+$) cells. **c**, E13.5 and E14.5 Ly6A-GFP anlagen lymph nodes were stained with GFP, IL-7Rα and Ki67 antibodies and analysed by confocal microscopy. **d**, E14.5 *Rorgt*$^{-/-}$ mesenteric lymph nodes were stained with podoplanin, IL-7Rα and CD45 antibodies and analysed by confocal microscopy. **e**, Percentage of E16.5 ILC_{4neg} and LTi_4 cells gated in $CD45^+CD3^-CD11c^-$ determined by flow cytometry in *Rorgt*$^{+/+}$ and *Rorgt*$^{-/-}$ intestines. Data are representative of three independent experiments. **f**, Left: pregnant mice received RAR antagonist BMS493 or the vehicle DMSO from E10.5 until E13.5. The ratio LTi_4/ILC_{4neg} cells in the fetal liver was determined at E13.5; $n = 8$. Right: pregnant mice received BMS493 or the vehicle DMSO. Frequency of colonizing haematopoietic cells was determined in E17.5 intestines by flow cytometry; $n = 4$. **g**, Pregnant *hCD2*-GFP mice were administered BMS493 or DMSO from E10.5 until E13.5. Embryos were analysed at E17.5; $n = 13$. Arrowheads show anlagen lymph nodes. Scale bars: 50 μm (**c**, **d**); 500 μm (**g**). Error bars show s.e. Two-tailed *t*-test *P* values are indicated. $^*P < 0.05$; $^{**}P < 0.01$; $^{***}P < 0.001$. NS, not significant.

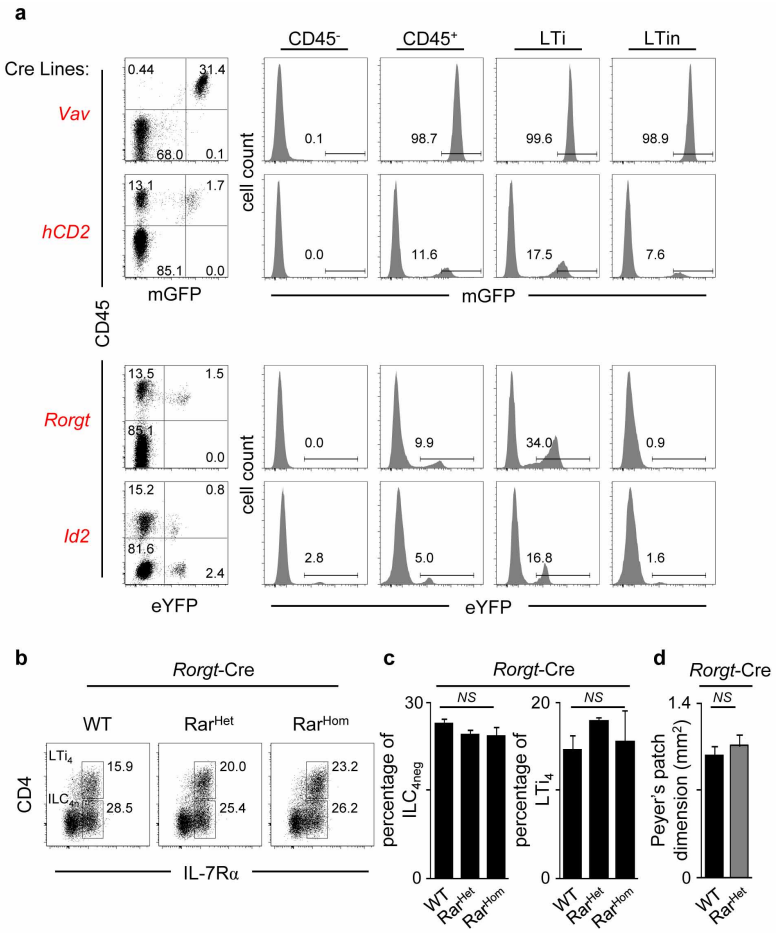

Extended Data Figure 2 | Analysis of mouse haematopoietic-cell-specific Cre lines. **a**, *Vav*-iCre and *hCD2*-Cre mice were crossed with *ROSA26*-Tomato-mGFP mice. *Rorgt*-Cre and *Id2*-CreERT2 mice were crossed with *ROSA26*-eYFP mice. E15.5 intestines were analysed by flow cytometry. Left: results show the percentage of mGFP or eYFP positive cells in gut cell suspensions. Right: percentage of mGFP or eYFP positive cells in non-haematopoietic ($CD45^-$), haematopoietic ($CD45^+$), LTi and LTin cells. Results are representative of three independent experiments. **b**, Percentage of enteric E15.5 ILC_{4neg} and LTi_4 cells determined by flow cytometry in wild-type, *Rorgt*-Cre Rar^{Het} and *Rorgt*-Cre Rar^{Hom} littermates. **c**, Frequencies of enteric ILC_{4neg} and LTi_4 cells in wild-type, *Rorgt*-Cre Rar^{Het} and *Rorgt*-Cre Rar^{Hom} littermates. WT, $n = 5$; *Rorgt*-Cre Rar^{Het}, $n = 5$; *Rorgt*-Cre Rar^{Hom}, $n = 4$. **d**, Peyer's patch area at 6–7 weeks of age. WT, $n = 3$; *Rorgt*-Cre Rar^{Het}, $n = 4$. Two-tailed *t*-test *P* values are indicated. $^*P < 0.05$; $^{**}P < 0.01$; $^{***}P < 0.001$. NS, not significant.

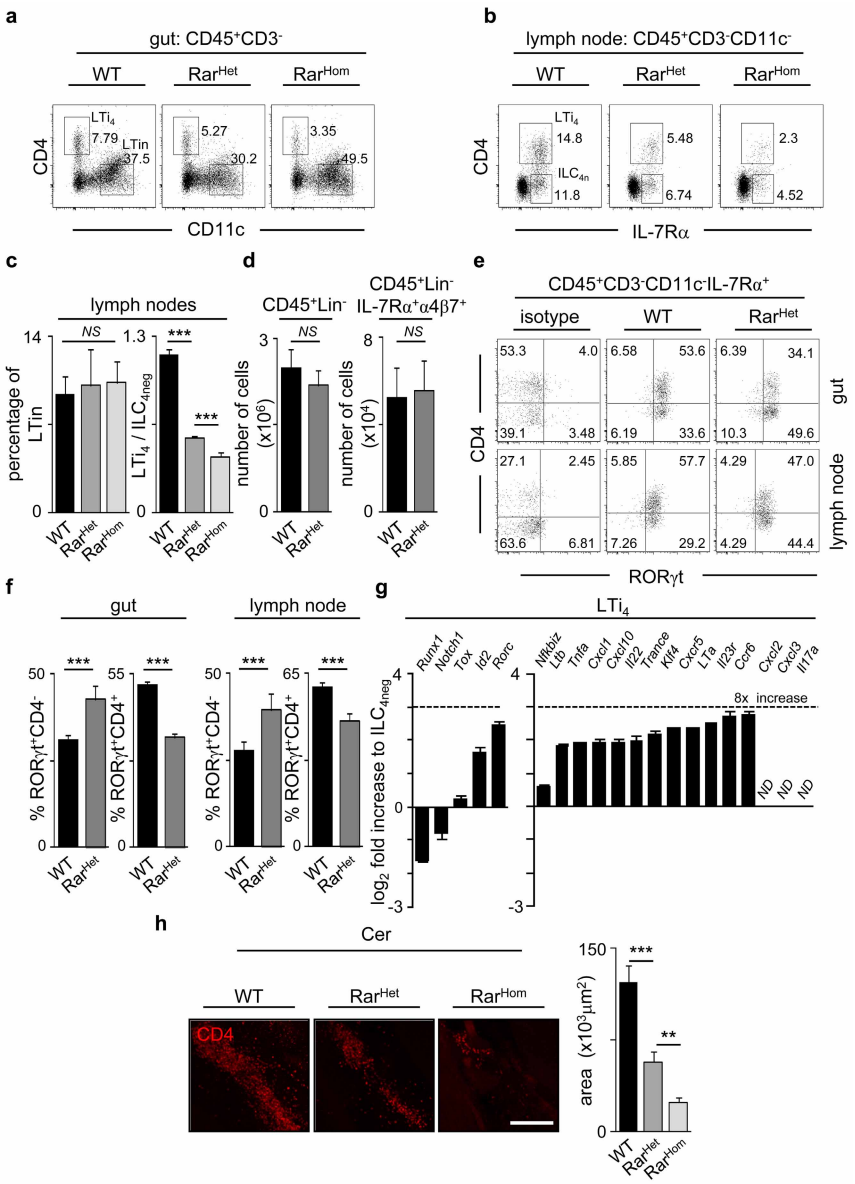

Extended Data Figure 3 | Analysis of *Vav*-iCre/*ROSA26*-RARα403 mice. **a**, E15.5 intestines from wild-type, *Vav*-iCre Rar^{Het} and Rar^{Hom} mice were analysed by flow cytometry. Representative analysis of six independent experiments is shown. **b**, E15.5 regions of cervical, brachial and inguinal lymph node from wild-type, *Vav*-iCre Rar^{Het} and Rar^{Hom} mice were analysed by flow cytometry. Representative analysis of two independent experiments. **c**, LTin cell percentage and LTi_4/ILC_{4neg} cell ratios are shown in E15.5 lymph nodes; $n = 4$. **d**, E15.5 fetal livers from wild-type and *Vav*-iCre Rar^{Het} mice were analysed by flow cytometry. Results show number of $CD45^+Lin^-$ ($n = 4$) and $CD45^-Lin^-IL\text{-}7R\alpha^+\alpha4\beta7^+$ progenitors ($n = 3$). **e**, Percentage of $CD45^+CD3^-CD11c^-IL\text{-}7R\alpha^+ROR\gamma t^+CD4^-$ ($ROR\gamma t^+CD4^-$) and $CD45^+CD3^-CD11c^-IL\text{-}7R\alpha^+ROR\gamma t^+CD4^+$ ($ROR\gamma t^+CD4^+$) cells determined by flow cytometry in RAR^{Het} and wild-type littermate controls in E15.5 guts and lymph nodes. **f**, Frequencies of $ROR\gamma t^+CD4^-$ and $ROR\gamma t^+CD4^+$ cells in mice described in **e**; WT, $n = 9$; Rar^{Het}, $n = 3$. **g**, ILC_{4neg} cells were purified from E15.5 wild-type intestines by flow cytometry and cultured for 6 days. LTi_4 cells raised *in vitro* were purified by flow cytometry and quantitative RT–PCR analysis performed. Results show $\log_2$ fold increase in comparison to their cultured ILC_{4neg} cell counterparts. Results were normalized to *Hprt1* and *Gapdh*. **h**, Left: E15.5 embryos were whole-mount stained for CD4 (red) and imaged by confocal microscopy. Cervical (Cer) lymph nodes are shown. Right: cervical lymph node dimensions are shown. WT, $n = 5$; Rar^{Het}, $n = 7$; Rar^{Hom}, $n = 6$. Scale bar: 50 μm. Two-tailed *t*-test *P* values are indicated. $^*P < 0.05$; $^{**}P < 0.01$; $^{***}P < 0.001$. NS, not significant. ND, not detected.

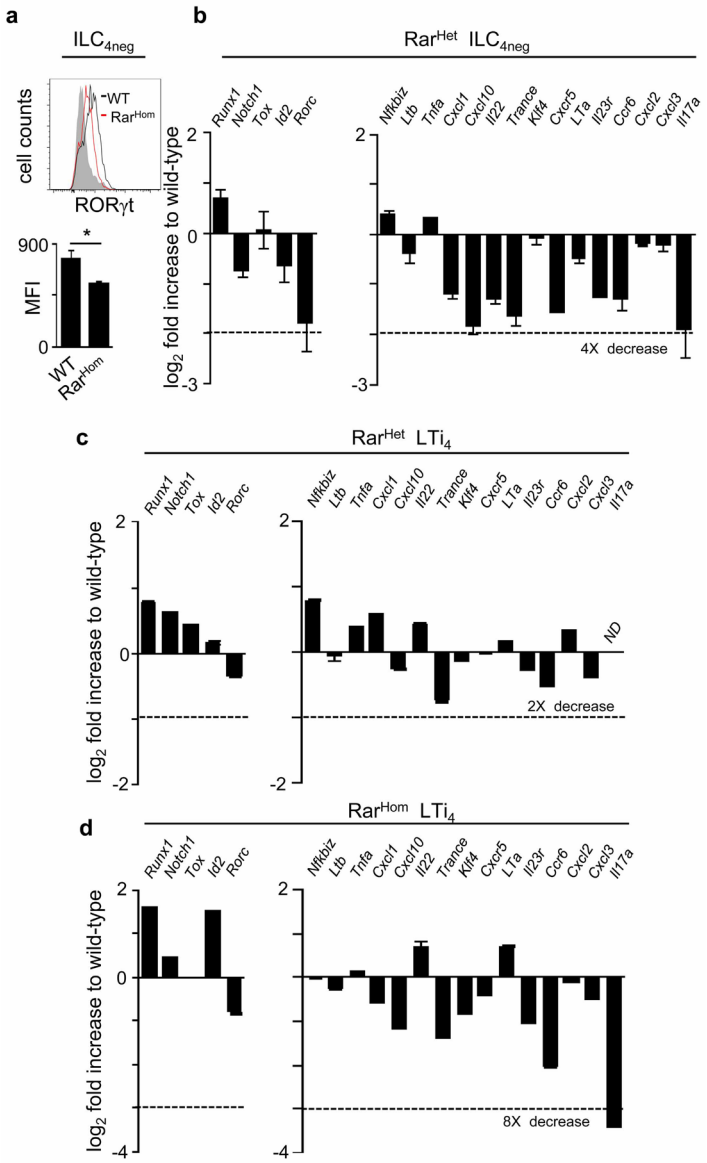

Extended Data Figure 4 | Gene expression patterns in ILC_{4neg} and LTi_4 cells. **a**, E15.5 intestines from Rar^{Hom} and wild-type littermate controls were brought to suspension and analysed by flow cytometry. Upper panel: RORγt expression. Lower panel: mean fluorescence intensity of RORγt expression in ILC_{4neg} cells; $n = 3$. **b**, ILC_{4neg} cells were purified from E15.5 Rar^{Het} and wild-type littermate control intestines and lymph nodes. Quantitative RT–PCR analysis was performed. Results show $\log_2$ fold increase to wild type. Results were normalized to *Hprt1* and *Gapdh*. Results from three independent measurements are shown. **c**, **d**, LTi_4 cells were purified from E15.5 Rar^{Het} (**c**), Rar^{Hom} (**d**) and wild-type littermate control intestines and lymph nodes. Quantitative RT–PCR analysis was performed. Results show $\log_2$ fold increase to wild type. Results were normalized to *Hprt1* and *Gapdh*. Data from three independent measurements are shown. Two-tailed *t*-test *P* values are indicated. $*P < 0.05$; $**P < 0.01$; $***P < 0.001$. ND, not detected.

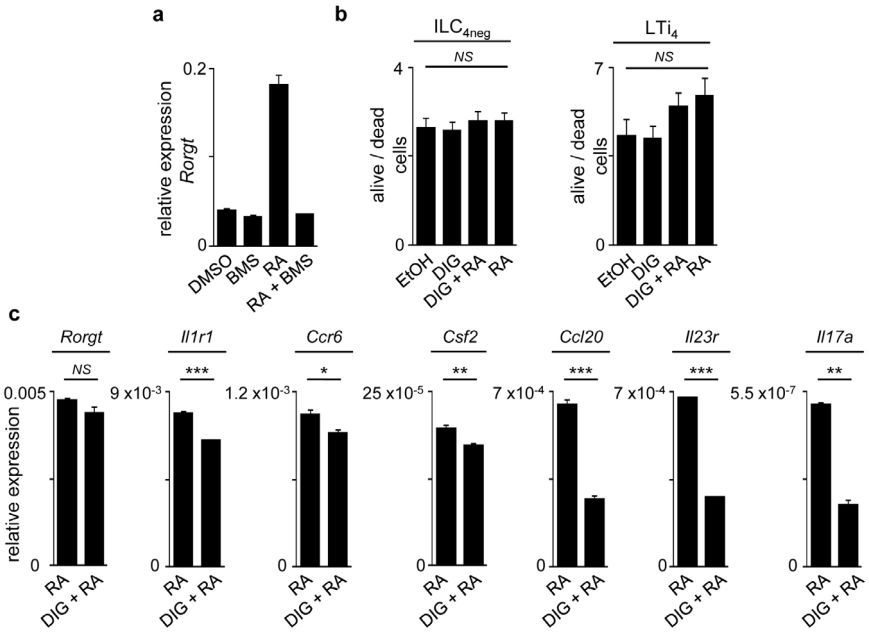

Extended Data Figure 5 | Treatment of ILC_{4neg} and LTi_4 cells with digoxin. **a**, Wild-type ILC_{4neg} cells were FACS purified, starved overnight and stimulated with DMSO, BMS493 (100 nM), RA (100 nM) and RA plus BMS493 (100 nM each) for 16 h. Results show quantitative RT–PCR analysis normalized to *Gapdh*; $n = 3$. **b**, E13.5 lymph node cell suspensions were cultured with vehicle (ethanol), digoxin, digoxin + RA and RA alone for 24 h. Alive/dead cell ratios were determined by flow cytometry and DAPI staining; $n = 4$. **c**, ILC_{4neg} cells were isolated from wild-type E15.5 embryos starved overnight and stimulated for 6 h in the presence of RA (100 nM) or DIG (10 μM) + RA (100 nM). Results show quantitative RT–PCR analysis of *Rorgt* and RORγt downstream targets normalized to *Gapdh*. Representative of three independent experiments. Error bars show s.e. Two-tailed *t*-test *P* values are indicated. $*P < 0.05$; $**P < 0.01$; $***P < 0.001$. NS, not significant.

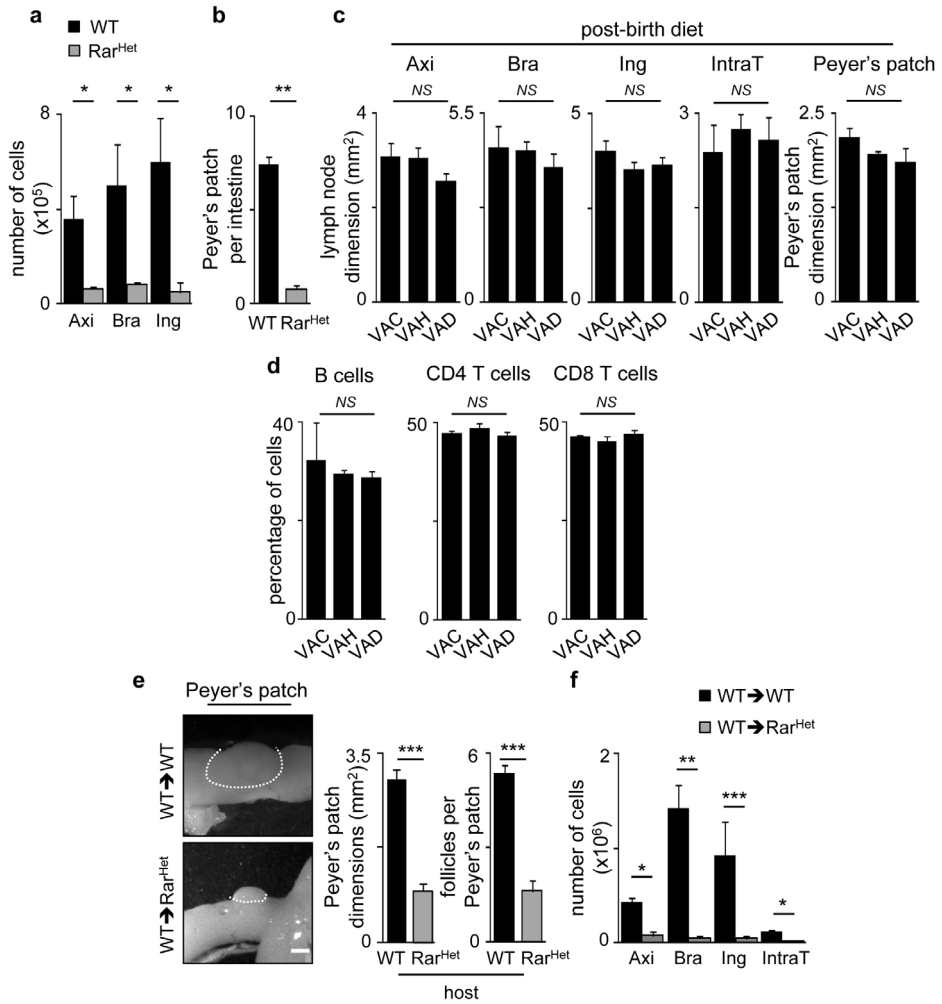

Extended Data Figure 6 | Analysis of SLOs from adult mice with variable RA signalling levels. **a**, Axillary (Axi), brachial (Bra) and inguinal (Ing) lymph nodes from adult Rar^{Het} and wild-type littermate controls were analysed. Results show lymph node cell numbers; $n = 6$. **b**, Results show Peyer's patch number per intestine from adult Rar^{Het} and wild-type littermate controls; $n = 6$. **c**, Six-week-old wild-type females received VAC, VAH or VAD ($n = 3$) diet for 7 weeks. Axillary (Axi), brachial (Bra), inguinal (Ing), intrathoracic (IntraT) lymph nodes and Peyer's patches (PP) dimensions were analysed; $n = 3$. **d**, Percentage of $CD45^+CD19^+$ B cells; $CD4^+$ and $CD8^+$ T cells in inguinal lymph nodes; $n = 3$. **e**, **f**, Two-week-old CD45.2 Rar^{Het} and wild-type littermate controls were lethally irradiated and transplanted with wild-type CD45.1 bone marrow cells. Chimaeric mice were analysed 8 weeks after reconstitution. **e**, Results show Peyer's patch dimensions and follicle number/Peyer's patch; $n = 6$. **f**, Results show number of cells in axillary (Axi), brachial (Bra) inguinal (Ing) and intrathoracic (IntraT) lymph nodes; $n = 6$. Scale bar: 1 mm. Error bars show s.e. Two-tailed *t*-test *P* values are indicated. $^*P < 0.05$; $^{**}P < 0.01$; $^{***}P < 0.001$. NS, not significant.

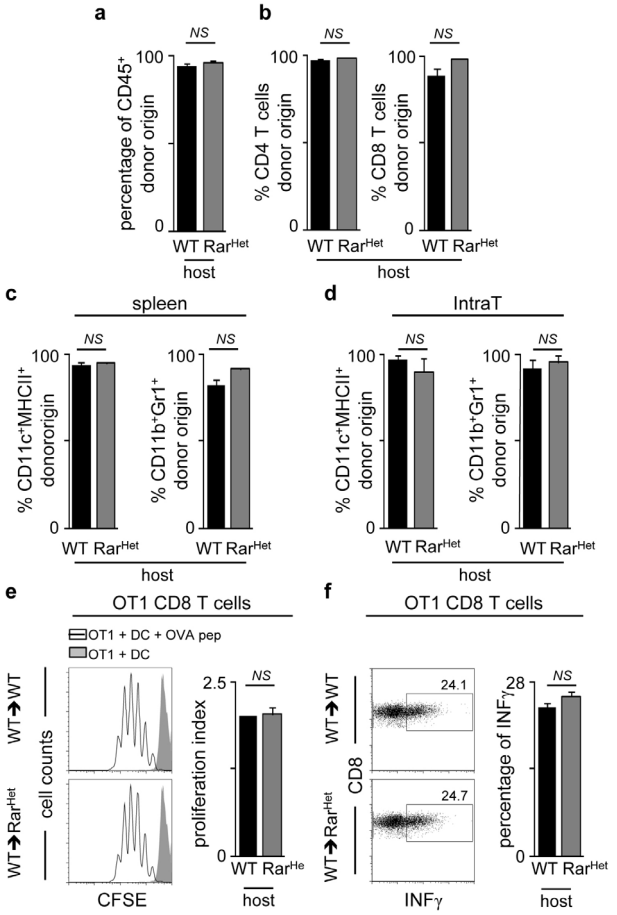

Extended Data Figure 7 | Analysis of WT→WT and WT→Rar^{Het} bone marrow chimaeras. Two-week-old CD45.2 Rar^{Het} and wild-type littermate controls were lethally irradiated and transplanted with wild-type CD45.1 bone marrow cells. Chimaeric mice were analysed 8 weeks after reconstitution. **a**, Reconstitution of donor CD45.1 cells in WT→WT and WT→Rar^{Het} chimaeras in the spleen ($n = 4$). **b**, Reconstitution of donor CD45.1 CD4 and CD8 T cells in WT→WT and WT→Rar^{Het} chimaeras in the spleen. WT→WT, $n = 4$; WT→Rar^{Het}, $n = 11$. **c**, Reconstitution of donor CD45.1 CD11c^{+}MHCII^{+} and CD11b^{+}Gr1^{+} myeloid cells in WT→WT and WT→Rar^{Het} chimaeras in the spleen; $n = 3$. **d**, Reconstitution of donor CD45.1 CD11c^{+}MHCII^{+} and CD11b^{+}Gr1^{+} cells in WT→WT and WT→Rar^{Het} chimaeras in intrathoracic lymph nodes; $n = 3$. **e**, Dendritic cells (DCs) were purified from WT→WT and WT→Rar^{Het} chimaeras. Dendritic cells were loaded with OVA peptide (10^{-5} μM) and co-cultured for 3 days with CFSE-labelled monoclonal OT1 CD8 T cells. OT1 CD8 T-cell proliferation was analysed by CFSE dilution. Proliferation index is shown. WT, $n = 4$; Rar^{Het}, $n = 6$. **f**, Dendritic cells were purified from WT→WT and WT→Rar^{Het} chimaeras. Dendritic cells were loaded with OVA peptide (10^{-5} μM) and co-cultured for 3 days with OT1 CD8 T cells. Percentage of IFN-γ-producing OT1 CD8 T cells is shown; $n = 4$. Error bars show s.e. Two-tailed *t*-test *P* values are indicated. $*P < 0.05$; $**P < 0.01$; $***P < 0.001$. NS, not significant.

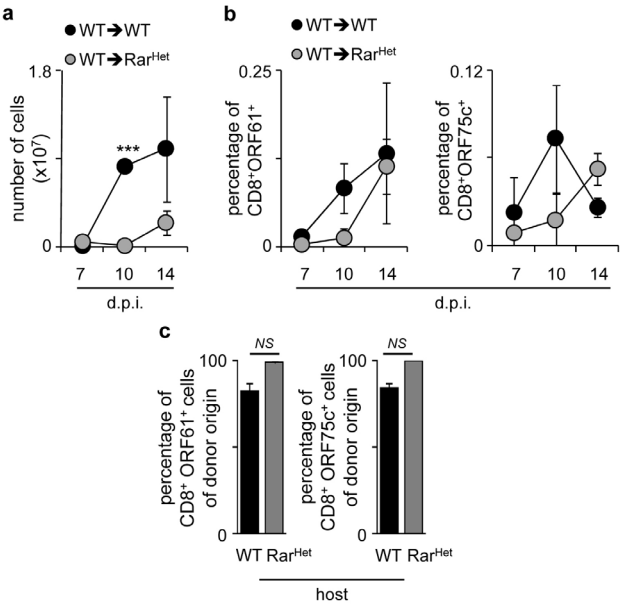

Extended Data Figure 8 | Infection of WT→Rar^{Het} or WT→WT chimaeras with murid herpesvirus-4. **a**, Intrathoracic lymph node cellularity in WT→WT and WT→Rar^{Het} chimaeras at different days post-infection (d.p.i.). WT, $n = 5$; Rar^{Het}, $n = 3$. **b**, Percentage of CD8$^+$ORF61$^+$ (left) and ORF75c$^+$ (right) T cells in intrathoracic lymph nodes at different days post-infection (d.p.i.). WT, $n = 5$; Rar^{Het}, $n = 3$. **c**, Percentage of donor CD45.1 CD8$^+$ORF61$^+$ (left) and CD8$^+$ORF75c$^+$ (right) T cells in WT→WT and WT→Rar^{Het} chimaeras after infection with murid herpesvirus-4. WT, $n = 6$; Rar^{Het}, $n = 12$. Error bars show s.e. Two-tailed *t*-test *P* values are indicated. $^*P < 0.05$; $^{**}P < 0.01$; $^{***}P < 0.001$. NS, not significant.

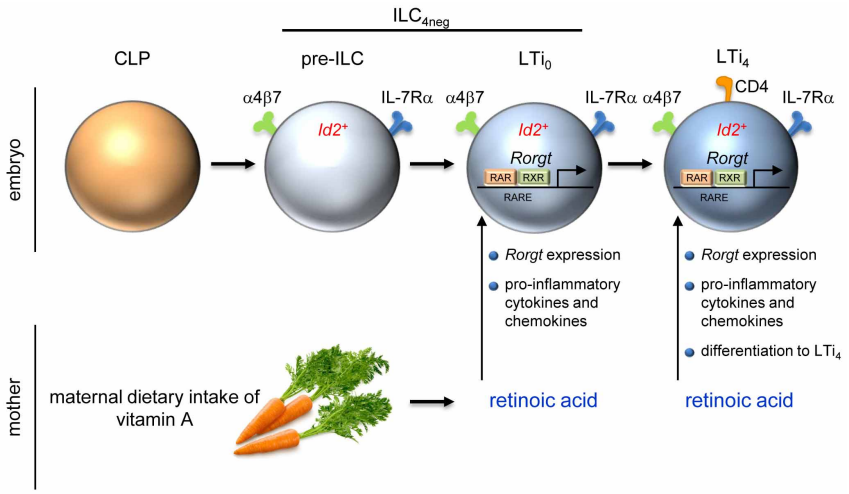

Extended Data Figure 9 | Impact of maternal retinoids in ILC3s. Maternal dietary intake of vitamin A is catabolized into bioactive retinoic acid (RA). RA signals control type 3 innate lymphoid cells (ILC3) in the embryo. Fetal ILC3s include ILC_{4neg} and LTi_4 cells. LTi_4 cells are $Id2^+ROR\gamma t^+$, whereas enteric ILC_{4neg} cells contain a minor subset of $Id2^+ROR\gamma t^-$ cells (pre-ILCs). RA signalling operates in a cell-autonomous fashion, via direct regulation of *Rorgt*, programming innate pro-inflammatory cytokines and chemokines and differentiation of LTi_4 cells.

Extended Data Table 1 | Computational analysis of putative RARE sites in the *Rorc* locus

Site ID	Primer Sequences	Putative RARE Sites	Position	TESS Sequence entry	TESS Factor
A	TGAAGCAGCTAGTCACTTCC CAGCTCTCCAGCTTGTATTG	GAGGAGCAGGG	-7,837 *Rorg* TSS	GAGGtCAGGG	T00721 RAR-beta T01334 RXR-beta
B	GAAACTTTATCTGGGGCTGG TGAACTCAGGAAGAGCAGCA	GGTTCAGAGGT	-7,446 *Rorg* TSS	GGTTCA	T00721 RAR-beta
				GGTTCAGAGGT	I00038 (RXR-alpha)
C	AACCTGGCACTTCGCACTTAA GAGTGGGCGGACTTCTCAGA	TGAACT	-5,478 *Rorg* TSS	TGAACT	T00721 RAR-beta
D	GAGGCCTCTAAGTACCGCCATT CGCCCTGAATCCTGTCACA	AGGTCAGCACCA	-4,690 *Rorg* TSS	AGGTCA	T00721 RAR-beta
				AGGTCA	_00000 RAR-beta
				AGGTCAGCACCA	T00719 RAR-alpha1 T01345 RXR-alpha
E	CAGAGATGACCTAGTCAGTGGAGTACTG ACCCCCCAAAACCCTTGA	GGGGTCAAGGGT TGACCT	-1,800 *Rorg* TSS	GGGTCA	T00719 RAR-alpha1 T00720 RAR-gamma T00721 RAR-beta T01329 RAR-gamma
				GGGTCA	_00000 RAR-beta
				GGGGTCA	T01331 RXR-alpha T01332 RXR-beta
				GGGTCA	T00719 RAR-alpha1 T00720 RAR-gamma T00721 RAR-beta T01329 RAR-gamma
				TGACCT	_00000 RAR-beta
				GGGTCAAGGGT	_00000 RXR-alpha
				GGGTCA	T00721 RAR-beta
				TGACCT	T00721 RAR-beta
F	ACCACTGAGCCATCTCTCCTACC TTTTGTGATGTGGGTTCTGGG	GGGTCA	-1,638 *Rorg* TSS	GGGTCA	T00719 RAR-alpha1 T00720 RAR-gamma T00721 RAR-beta T01329 RAR-gamma
				GGGTCA	_00000 RAR-beta
				GGGTCA	T00721 RAR-beta
G	GACAATCTCATCAGAGGAGG GGGCAACCAATGAGTATGTG	TCACCTCT	-1,619 *Rorgt* TSS	TCACCTC	_00000 RAR-gamma

Computational analysis was performed using TESS (Transcription Element Search System) (http://www.cbil.upenn.edu/tess). TSS (*Rorg*), ACGGGCCAGGTGCTCCCTCC; TSS (*Rorgt*), AGAAACACTGGGGGAGAGCTTTG.